Interdecadal change of the boreal summer circumglobal teleconnection (1958–2010)

Hong Wang,[1,2] Bin Wang,[2] Fei Huang,[1] Qingua Ding,[3] and June-Yi Lee[2]

Received 14 May 2012; accepted 31 May 2012; published 26 June 2012.

[1] The tropical-extratropical teleconnection during boreal summer is characterized by a circumglobal teleconnection (CGT) pattern in the northern hemisphere (NH). Around the late 1970s, there was an abrupt change in the coupled atmosphere-ocean system over the NH and global tropics. This study found that the CGT has experienced a significant change since late 1970s. During the recent epoch (1979-2010), the major CGT centers weakened with pronounced changes over the North Atlantic and Europe. Partial correlation analysis of 200-hPa geopotential height and the NH summer monsoon heat sources indicates that the change of Indian summer monsoon (ISM) rainfall has a global impact on the CGT, whereas other NH summer monsoons (West African, western North Pacific, and North American) have only a regional modification to the CGT. The weakening of the CGT pattern in the recent epoch is a consequence of weakened coupling between ISM rainfall and midlatitude circulation, which results from the reduced interannual variability of ISM rainfall due to changes in El Niño-Southern Oscillation properties. The large change of the CGT over the North Atlantic and Europe is attributed to a southward shift of upper-level westerlies and enhanced coupling to West African monsoon rainfall. **Citation:** Wang, H., B. Wang, F. Huang, Q. Ding, and J.-Y. Lee (2012), Interdecadal change of the boreal summer circumglobal teleconnection (1958–2010), *Geophys. Res. Lett.*, *39*, L12704, doi:10.1029/2012GL052371.

1. Introduction

[2] Based on an analysis of 56-year (1948-2003) monthly mean anomaly data during boreal summer, *Ding and Wang* [2005, hereinafter DW05] identified a circumglobal teleconnection (CGT) pattern in the northern hemisphere (NH). Interannually, the CGT tends to couple with the Indian summer monsoon (ISM) rainfall variability and appear preferentially in summers preceding the peak phases of El Niño-Southern Oscillation (ENSO) cycle [*Ding et al.*, 2011].

[3] The CGT links regional teleconnection patterns, including a) ISM-East Asian summer monsoon (EASM) teleconnection [*Krishnan and Sugi*, 2001], b) an Eurasian teleconnection pattern oriented along the westerly jet stream [*Joseph and Srinivasan*, 1999], and c) the Western North Pacific (WNP)-North American teleconnection [*Lau and Weng*, 2002]. The boreal summer CGT pattern has been the topic of subsequent investigations focusing on meteorological aspects [*Ding and Wang*, 2007] and climatic aspects [*Lin*, 2009; *Yasui and Watanabe*, 2010]. Although the boreal summer teleconnection is weaker than its winter counterpart, it is intimately coupled to surface air temperature and precipitation variability in the NH extratropics [*Ding et al.*, 2011] and may act as a significant source of climate predictability over the extratropical region of interest [*Wang et al.*, 2008b; *Lee et al.*, 2010, 2011].

[4] It has been well recognized that an abrupt climate regime shift occurred in the late 1970s, which involved a global-scale change in SST over the Pacific and Atlantic and the associated atmospheric teleconnection pattern [*Nitta and Yamada*, 1989; *Trenberth*, 1990]. In particular, the ENSO property including period, amplitude, spatial structure, and propagation has been changed [*Wang*, 1995; *An and Wang*, 2000], and the ENSO-ISM relationship has weakened [*Kumar et al.*, 1999] but the ENSO-WNP/EASM relationship strengthened [*Wang et al.*, 2008a]. A natural question arises as to whether the tropical-extratropical teleconnection has been changed associated with this global climate regime shift. This paper aims to address this question.

2. Data and Method

[5] The datasets used include 1) monthly global SST for the period 1958-2010 from the NOAA extended reconstructed SST (ERSST) version 3 [*Smith et al.*, 2008]; 2) the NOAA global monthly precipitation reconstruction (PREC) dataset [*Chen et al.*, 2004]; 3) the monthly land surface air temperature dataset compiled by the Climatic Research Unit (CRU) [*Mitchell and Jones*, 2005], and 4) a combined ECMWF ERA-40 and ERA-interim dataset for geopotential heights and winds [*Uppala et al.*, 2005, 2008]. The ERA-40 Re-analysis 2.5° × 2.5° monthly data (1958-1998) and ERA-interim 1.5° × 1.5° monthly data (1989-2010) were interpolated onto the same 2.5° × 2.5° grid points. To focus on year-to-year variations, the decadal variations with periods longer than 8 years were removed using Fourier harmonic analysis of the seasonal mean (June through September, JJAS) anomalies.

[6] The maximum covariance analysis (MCA) was used to capture the dominant coupled patterns between the NH 200-hPa geopotential height (H200) and tropical precipitation (a

[1]Physical Oceanography Laboratory and Joint Open Laboratory of Marine Meteorology, Ocean University of China, Qingdao, China.
[2]International Pacific Research Center, School of Ocean and Earth Science and Technology, University of Hawaii at Manoa, Honolulu, Hawaii, USA.
[3]Department of Earth and Space Sciences and Quaternary Research Center, University of Washington, Seattle, Washington, USA.

Corresponding author: F. Huang, Physical Oceanography Laboratory, Ocean University of China, Qingdao 266003, China. (huangf@ouc.edu.cn)

0094-8276/12/2012GL052371

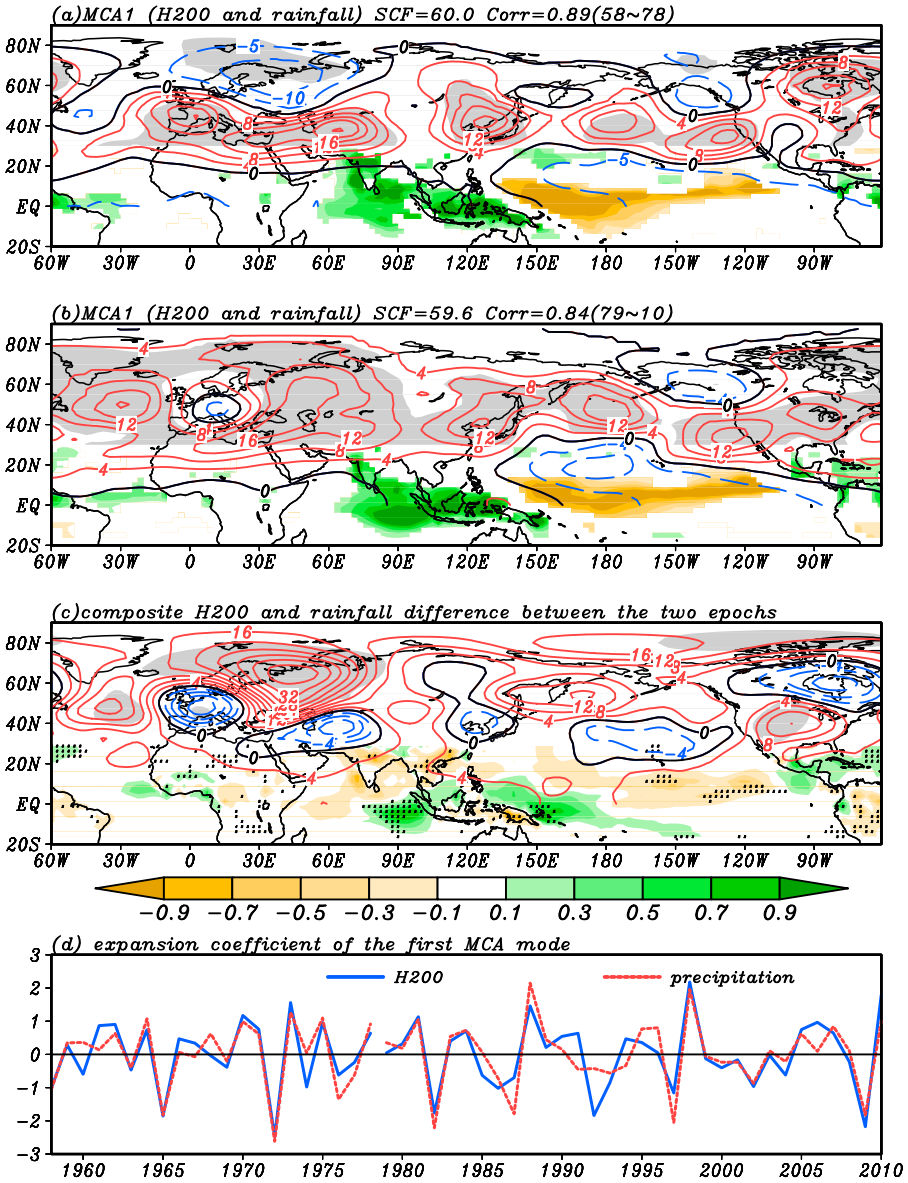

Figure 1. The first MCA mode of summer (JJAS) H200 (contours, interval 4 m) and tropical rainfall (15°S∼30°N, color shading, units: 1 mm/day): (a) for 1958∼1978 period, (b) for 1979∼2010 period. (c) The difference of composited fields for H200 and rainfall between the two epochs. The grey shading denotes homogeneous (or heterogeneous) correlations that are significant at or above the 90% confidence level for Figures 1a and 1b. The grey shading in Figure 1c denotes the area that the composited H200 field difference between two epochs is above 90% confidence level (only over the regions north of 30°N has been showed). Dots mark the rainfall difference above the 90% confidence level. (d) The expansion coefficient of MCA1 (blue solid line for H200 and red dash line for precipitation). The squared covariance fraction (SCF) and the temporal correlation coefficient (Corr.) between two expansion coefficients are indicated on the top of each panel.

measure of the tropical forcing) [*Wallace et al.*, 1992]. Square root of cosine of latitude weighting was used in computing the covariance matrix.

3. Interdecadal Change of CGT

[7] Figure 1 shows the interdecadal changes of teleconnection pattern around the late 1970s. During 1958-1978, the belt-shape CGT around 40°N is clear with six well defined centers located at West Europe, central Asia, northeastern Asia, the central North Pacific, the eastern North Pacific, and eastern Canada (Figure 1a). During 1979-2010, the CGT pattern was weakened. Further, remarkable change of the anomaly pattern is found over the North America-Atlantic-Europe sector (Figure 1b). Student t-test for differences of composited H200 between two epochs (Figure 1c) indicates that changes were significant over the North Atlantic and northern Europe, and central North America.

[8] The tropical precipitation field associated with the CGT during the two epochs shows a significant southeastward shift over the warm pool and South Asia-WNP monsoon regions during the second epoch (Figure 1c). Precipitation was suppressed over the ISM region and Southeast Asia, but

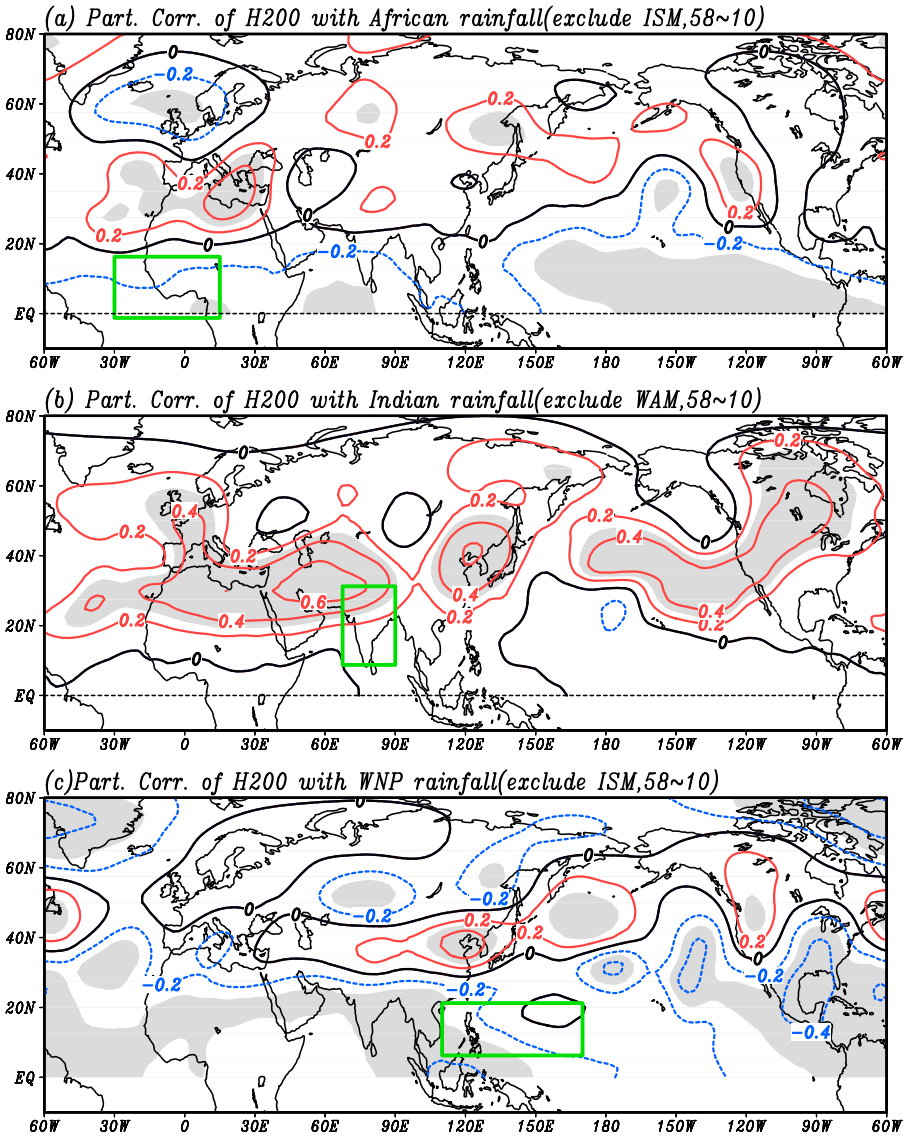

Figure 2. Partial correlation maps between summer (JJAS) H200 and regional monsoon rainfall for the period of 1958-2010: (a) West African Monsoon, (b) Indian Monsoon and (c) WNP monsoon. The green box indicates the area over which the rainfall rate was averaged for each monsoon region. The grey shading donates the area that the partial correlation coefficient is statistically significant at the 90% confidence level.

enhanced over the equatorial western Pacific and other NH summer monsoon regions (WNP, West African and Mexican monsoon regions).

[9] Changes are also noticed in the time series of the expansion coefficient of the first MCA mode in Figure 1d. The interannual variability of the expansion coefficient has larger amplitude and longer periodicity during the second epoch than the first.

4. Possible Reasons for the Interdecadal Change of CGT

[10] In theory, change of the coupled teleconnection pattern can be directly caused by change of tropical precipitation (latent heat) pattern or change of mean background circulation (basic flows), especially the jet stream structure and the boundaries between midlatitude westerly and tropical easterly [*Hoskins and Ambrizzi*, 1993]. Because summer monsoon precipitation is located close to the upper-level westerlies, change of monsoon should have strong influence on the teleconnection pattern even if the midlatitude basic state is unchanged. In reality, the two factors are working in union.

[11] To see the linkages between various monsoon precipitation anomalies and midlatitude wavetrain patterns, Figure 2 presents the teleconnection patterns associated with each monsoon precipitation anomaly as hinted by partial correlation maps. In view of the dominant influence of Indian monsoon, the partial correlations calculated for West African and WNP precipitation have removed the influence of ISM. Similarly, in view of the downstream impact of the monsoon heat source, the calculation of the partial correlation for ISM has removed potential influence of West African monsoon (WAM). The ISM precipitation is associated with the entire CGT pattern (Figure 2b). In sharp contrast, the African monsoon precipitation is primarily linked with

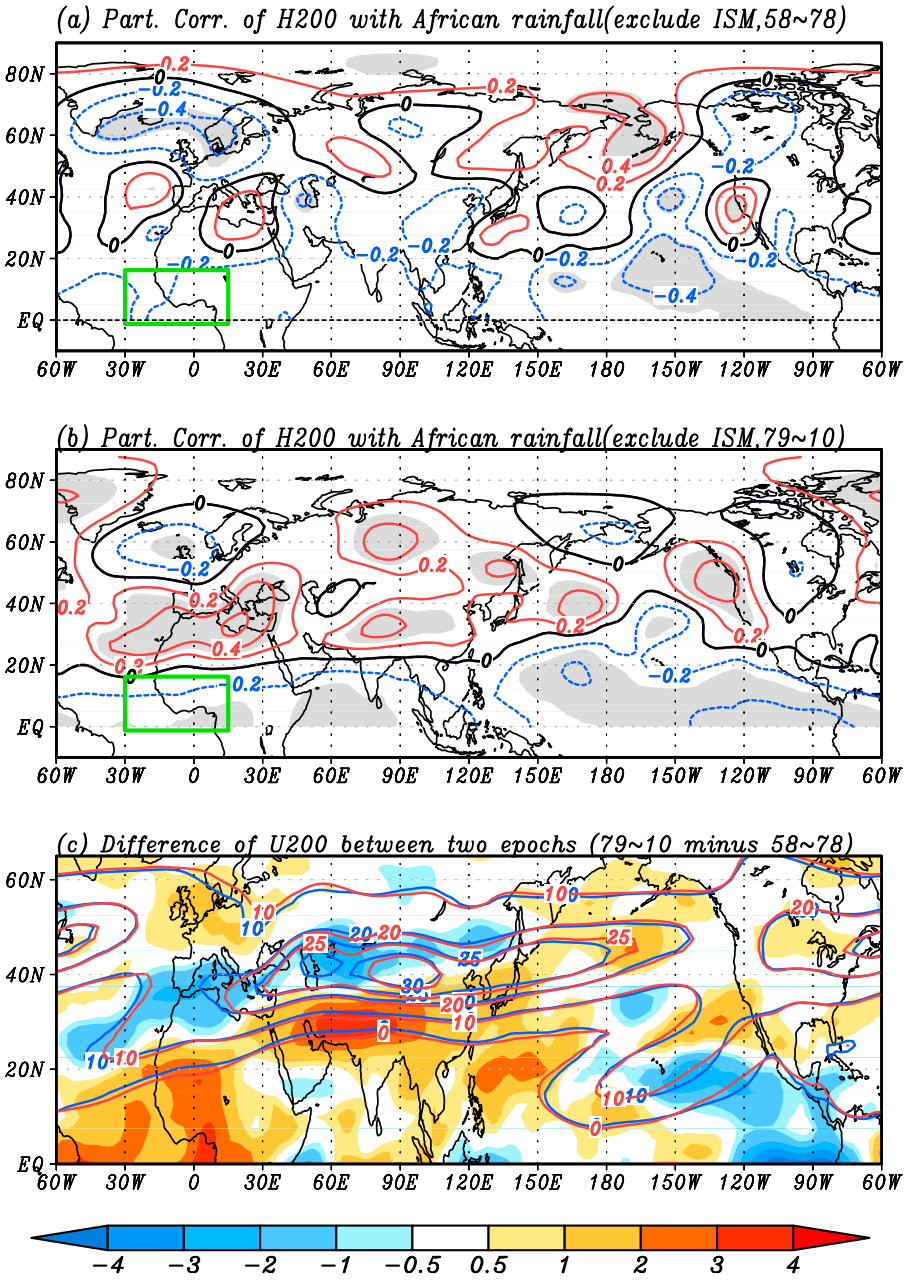

Figure 3. The partial correlation maps between West African summer monsoon rainfall and H200 in (a) 1958-1978 and (b) 1979-2010 epoch. Green box indicate the monsoon area. The grey shading donates the area that the correlation coefficient is statistically significant at the 90% confidence level, 0.37 for 1958∼1978 period and 0.30 for 1979∼2010 period. (c) The difference of summer mean 200 hPa zonal wind between the two epochs (1979∼2010 minus 1958∼1978, shading) and the westerly speeds (contour, blue denotes 1958∼1978 mean and red the 1979∼2010 mean).

midlatitude anomalies over the North Atlantic and Western Europe (Figure 2a); and the WNP precipitation anomalies are principally connected to the midlatitude anomalies over East Asia and the northwestern Pacific (Figure 2c). The Mexican monsoon precipitation has a local correlation with the eastern North Pacific (figure not shown). These partial correlation patterns provide useful hints for interpreting how change of the tropical precipitation pattern could impact the CGT during the two epochs.

[12] The ISM has a global linkage with CGT because one of the key action centers of CGT, the subtropical central Asian high, is tightly coupled with Indian monsoon rainfall as evidenced by the baroclinic structure over the subtropical central Asia center (DW05). Enhanced ISM rainfall, especially over the northern India, tends to generate baroclinic Rossby wave response to its northwest [*Rodwell and Hoskins*, 1996].

[13] Why does the CGT weaken after the late 1970s? Based on the results shown in Figure 2, we argue that the major cause is the weakened ISM rainfall variability in the coupled pattern with the CGT. As shown in Figure 1, during the first epoch the ISM precipitation that coupled with the CGT was strong but in the recent decade it has decreased significantly (Figure 1c). Hence, the strong CGT pattern in

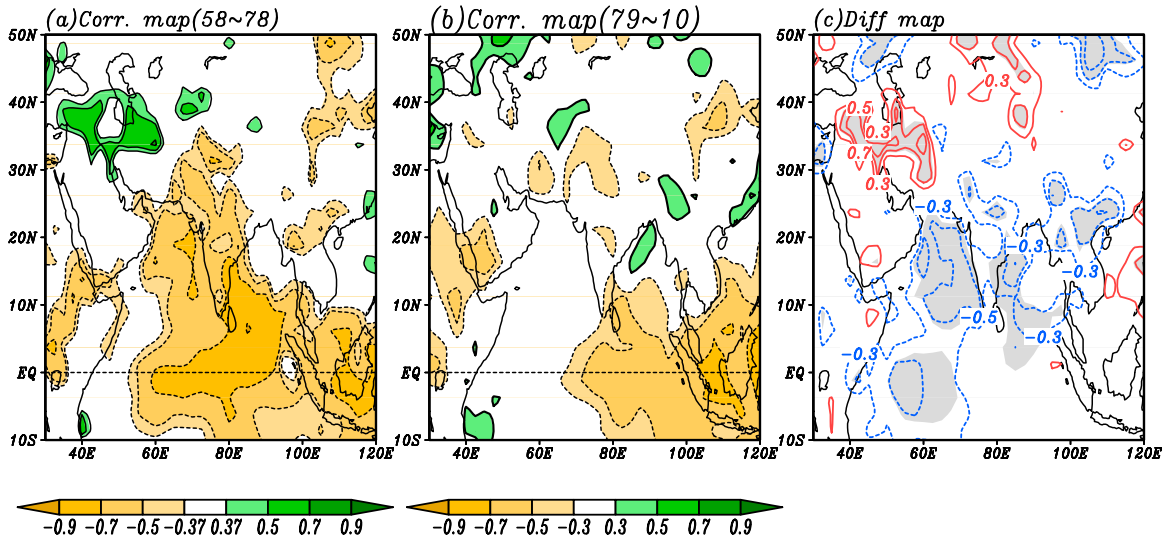

Figure 4. Correlation maps of JJAS rainfall with reference to Nino3 index for (a) 1958∼1978 period and (b) 1979∼2010 period. Only significant correlation coefficients exceeding 90% confidence level are plotted. (c) Difference map between Figures 4a an 4b (1958∼1978 minus 1979∼2010, contour). The regions where the correlation coefficients between the two epochs are statistically significant at 90% confidence level are shaded.

the first epoch (Figure 1a), which is similar to the pattern in Figure 2b, is a consequence of tight coupling between ISM and CGT, while the weakening of CGT during the second epoch results from the eastward shift of the tropical rainfall from India to the Philippine Sea in the coupled pattern (Figure 1c). We also argue that the mean flow change has a minor effect on the ISM-CGT coupling because the interdecadal change of jet stream over Asia is small (Figure 3c) and the heat source is already close to upper-level westerlies (figure not shown).

[14] Why has the teleconnection pattern dramatically changed over the Atlantic, Europe and North Africa? The partial correlation maps between the WAM precipitation and H200 during the two epochs are contrasted in Figures 3a and 3b. Both panels show a meridional dipole anomaly pattern over North Atlantic and Europe. However, during the first epoch, the high-latitude negative correlation was stronger, while the subtropical positive correlation was stronger and the dipole pattern shifted southward during the second epoch. This suggests a direct coupling between African monsoon rainfall and H200 subtropical anomaly has enhanced in the recent epoch. These changes in dipole pattern also influence downstream wave train activity through Rossby wave dispersion.

[15] The enhanced coupling between WAM rainfall and H200 is due to southward extension of the upper-level subtropical westerlies over North Africa (Figure 3c). Over the westerly jet entranced region (North Africa), the zonal wind at 200 hPa (U200) increases to the south of 20°N whilst decreases north of 20°N, implying the 200 hPa westerly wind increases and extends southward. This equatorward enhancement of westerlies north of the WAM region can enhance Rossby wave response associated with the WAM precipitation. Also noticed is the enhancement of the African monsoon precipitation in the coupled pattern during the recent decade (Figure 1c), which also favors for the change of CGT pattern over Atlantic and Europe.

[16] The WAM and internally-generated changes in the mean flow could be one source driving low-frequency variations in CGT. Recently, some new results reveal that both the summer NAO (SNAO) and the Atlantic Multidecadal Oscillation (AMO) show variability at decadal-interdecadal timescale [*Mariotti and Dell'Aquila*, 2012] and the atmospheric signatures associated with them resemble a circumglobal structure [*Bladé et al.*, 2011; *Msadek et al.*, 2011]. However, the time expansion of H200 almost does not correlate to SNAO and AMO in the two epochs.

[17] A deeper question is why the coupling between ISM and midlatitude wave trains has been weakened since the late 1970s? *Ding et al.* [2011] found that the CGT pattern preferably occurs during the developing summer of ENSO. ENSO affects the asymmetric component of CGT through changing ISM precipitation.

[18] Therefore, the correlation maps between Nino3 index and summer rainfall in the two epochs are examined (Figure 4). A salient difference between the two maps is found over ISM area. There was a significant negative correlation in the first epoch, but no significant correlation in the second epoch, suggesting that the ENSO-induced ISM anomaly has decreased. A substantial portion of the ISM variability comes from the ENSO effect. The weakened ISM-ENSO relationship implies a reduction in ISM variability. Therefore, the reduced summer monsoon variability weakened coupling between ISM and CGT.

5. Summary

[19] During the recent epoch, the major CGT teleconnection centers have been weakened with a prominent change over the North Atlantic and Europe. The weakening of the CGT is a consequence of weakened coupling between ISM rainfall and midlaititude circulation, which is caused by reduced Indian summer rainfall variability associated with the change of ENSO properties. The large change of CGT over the North Atlantic and European sector is due to

southward shift of upper level westerly jet and the enhanced coupling to North African monsoon rainfall. Further numerical experiments are needed to test these hypotheses.

[20] **Acknowledgments.** This study has been supported by Climate Dynamics Program of the National Science Foundation under award AGS-1005599, the National Basic Research Program of China (973 program 2012CB955604), the National Natural Science Foundation of China (grants 40975038 and 40830106), and the National Research Foundation of Korea (NRF) grant funded by the Korea government MEST (2011-0021927, GRL). This is SOEST publication 8685 and IPRC-892.

References

An, S.-I., and B. Wang (2000), Interdecadal change of the structure of the ENSO mode and its impact on the ENSO frequency, *J. Clim.*, *13*, 2044–2055, doi:10.1175/1520-0442(2000)013<2044:ICOTSO>2.0.CO;2.

Bladé, I., B. Liebmann, D. Fortuny, and G. J. van Oldenborgh (2011), Observed and simulated impacts of the summer NAO in Europe: Implications for projected drying in the Mediterranean region, *Clim. Dyn.*, doi:10.1007/s00382-011-1195-x.

Chen, M., P. Xie, J. E. Janowiak, and P. A. Arkin (2004), Verifying the reanalysis and climate models outputs using a 56-year data set of reconstructed global precipitation, paper presented at 14th AMS Conference on Applied Meteorology, Am. Meteorol. Soc., Seattle, Wash., 11–15 Jan.

Ding, Q.-H., and B. Wang (2005), Circumglobal teleconnection in the Northern Hemisphere summer, *J. Clim.*, *18*, 3483–3505, doi:10.1175/JCLI3473.1.

Ding, Q.-H., and B. Wang (2007), Intraseasonal teleconnection between the summer Eurasian wave train and the Indian monsoon, *J. Clim.*, *20*, 3751–3767, doi:10.1175/JCLI4221.1.

Ding, Q.-H., B. Wang, J. M. Wallace, and G. Branstator (2011), Tropical-extratropical teleconnections in boreal summer: Observed interannual variability, *J. Clim.*, *24*, 1878–1896, doi:10.1175/2011JCLI3621.1.

Hoskins, B. J., and T. Ambrizzi (1993), Rossby wave propagation on a realistic longitudinally varying flow, *J. Atmos. Sci.*, *50*, 1661–1671, doi:10.1175/1520-0469(1993)050<1661:RWPOAR>2.0.CO;2.

Joseph, P. V., and J. Srinivasan (1999), Rossby waves in May and the Indian summer monsoon rainfall, *Tellus, Ser. A*, *51*, 854–864, doi:10.1034/j.1600-0870.1999.00021.x.

Krishnan, R., and M. Sugi (2001), Baiu rainfall variability and associated monsoon teleconnection, *J. Meteorol. Soc. Jpn.*, *79*, 851–860, doi:10.2151/jmsj.79.851.

Kumar, K. K., B. Rajagopalan, and M. A. Cane (1999), On the weakening relationship between the Indian monsoon and ENSO, *Science*, *284*, 2156–2159, doi:10.1126/science.284.5423.2156.

Lau, K.-M., and H.-Y. Weng (2002), Recurrent teleconnection patterns linking summertime precipitation variability over East Asia and North America, *J. Meteorol. Soc. Jpn.*, *80*, 1309–1324, doi:10.2151/jmsj.80.1309.

Lee, J.-Y., et al. (2010), How are seasonal prediction skills related to models' performance on mean state and annual cycle?, *Clim. Dyn.*, *35*, 267–283.

Lee, J.-Y., et al. (2011), How predictable is the Northern Hemisphere summer upper-tropospheric circulation?, *Clim. Dyn.*, *37*, 1189–1203, doi:10.1007/s00382-010-0909-9.

Lin, H. (2009), Global extratropical response to diabatic heating variability of the Asian summer monsoon, *J. Atmos. Sci.*, *66*, 2697–2713, doi:10.1175/2009JAS3008.1.

Mariotti, A., and A. Dell'Aquila (2012), Decadal climate variability in the Mediterranean region: Roles of large-scale forcings and regional processes, *Clim. Dyn.*, *38*, 1129–1145, doi:10.1007/s00382-011-1056-7.

Mitchell, T. D., and P. D. Jones (2005), An improved method of constructing a database of monthly climate observations and associated high-resolution grids, *Int. J. Climatol.*, *25*, 693–712, doi:10.1002/joc.1181.

Msadek, R., C. Frankignoul, and Z. X. Li (2011), Mechanisms of the atmospheric response to North Atlantic multidecadal variability: A model study, *Clim. Dyn.*, *36*, 1255–1276, doi:10.1007/s00382-010-0958-0.

Nitta, T., and S. Yamada (1989), Recent warming of tropical sea surface temperature and its relationship to the Northern Hemisphere circulation, *J. Meteorol. Soc. Jpn.*, *67*, 375–383.

Rodwell, M. J., and B. J. Hoskins (1996), Monsoons and the dynamics of deserts, *Q. J. R. Meteorol. Soc.*, *122*, 1385–1404, doi:10.1002/qj.49712253408.

Smith, T. M., R. W. Reynolds, T. C. Peterson, and J. Lawrimore (2008), Improvements to NOAA's Historical Merged Land-Ocean Surface Temperature Analysis (1880–2006), *J. Clim.*, *21*, 2283–2296, doi:10.1175/2007JCLI2100.1.

Trenberth, K. E. (1990), Recent observed interdecadal climate changes in the Northern Hemisphere, *Bull. Am. Meteorol. Soc.*, *71*, 988–993, doi:10.1175/1520-0477(1990)071<0988:ROICCI>2.0.CO;2.

Uppala, S. M., et al. (2005), The ERA-40 reanalysis, *Q. J. R. Meteorol. Soc.*, *131*, 2961–3012, doi:10.1256/qj.04.176.

Uppala, S., D. Dee, S. Kobayashi, P. Berrisford, and A. Simmons (2008), Towards a climate data assimilation system: Status update of ERA-Interim, *ECMWF Newsl.*, *115*, 12–18.

Wallace, J. M., C. Smith, and C. S. Bretherton (1992), Singular value decomposition of wintertime sea surface temperature and 500-mb height anomalies, *J. Clim.*, *5*, 561–576, doi:10.1175/1520-0442(1992)005<0561:SVDOWS>2.0.CO;2.

Wang, B. (1995), Interdecadal changes in El Niño onset in the last four decades, *J. Clim.*, *8*, 267–285, doi:10.1175/1520-0442(1995)008<0267:ICIENO>2.0.CO;2.

Wang, B., J. Yang, T. Zhou, and B. Wang (2008a), Interdecadal changes in the major modes of Asian-Australian monsoon variability: Strengthening relationship with ENSO since the late 1970s, *J. Clim.*, *21*, 1771–1789, doi:10.1175/2007JCLI1981.1.

Wang, B., et al. (2008b), Advance and prospectus of seasonal prediction: assessment of the APCC/CliPAS 14-model ensemble retrospective seasonal prediction (1980–2004), *Clim. Dyn.*, *30*, 605–619, doi:10.1007/s00382-007-0310-5.

Yasui, S., and M. Watanabe (2010), Forcing processes of the summertime circumglobal teleconnection pattern in a dry AGCM, *J. Clim.*, *23*, 2093–2114, doi:10.1175/2009JCLI3323.1.